Shallow cumulus and congestus modes in circulating equilibria of the tropical atmosphere in a two-column model

L. Nuijens[a]*, K. Emanuel[b]

[a] *L. Nuijens, Geoscience and Remote Sensing Department, Delft University of Technology*
[b] *Department of Earth, Atmosphere and Planetary Sciences, Massachusetts Institute of Technology*

*Correspondence to: L. Nuijens, GRS/CITG, Delft University of Technology, PO-box 5048, 2600 GA Delft, the Netherlands. Email: louise.nuijens@tudelft.nl

Using a two-column radiative-convective equilibrium (RCE) model of an overturning circulation, we elucidate mechanisms that control convection in adjacent ascending and subsiding regions. The model numerically solves for two-dimensional non-rotating hydrostatic flow, which is damped by momentum diffusion in the boundary layer and model interior, and by convective momentum transport. Convection, clouds and radiative transfer are parameterized. From a state of RCE we incrementally lower the SST in one column, which collapses convection first to a congestus mode, and then to a shallow mode, with respective tops near 650-550 hPa and 850 hPa. The circulation that develops has mean descent over the cold ocean, which maximises near the congestus and shallow tops, where evaporative and radiative cooling are large. Compared to the shallow mode, the congestus mode occurs with a deeper moist layer and more precipitation, and hence less (radiative) cooling below cloud tops, enhanced stability near cloud base, a weaker circulation, and less deep convective precipitation in the ascending column. However, congestus, which extends well beyond the viscous boundary layer, only develops with ample momentum diffusion, which allows horizontal temperature gradients to persist in the presence of gravity waves. Congestus modes are thus absent when using small domains or no convective momentum transport. Congestus is halted below a dry layer with enhanced stability, which is near the freezing level. But instead of melting of ice, which is not represented in the model physics, the stable layer is created by the interaction of radiation with a humidity profile, which in turn is inherent to the models' mixing scheme. Our results show that radiation, momentum diffusion, convection, cloud microphysics, and the circulation are all important at setting the depth of convection in the subsiding column, and along with that, deep convection and precipitation in the ascending column.

Key Words: shallow cumulus; congestus; trimodal convection; circulations; radiative-convective equilibrium; two-column model

Received . . .

1. Introduction

Shallow convection has long been recognised as an important player in large-scale overturning circulations, in particular, in the Hadley circulation (Riehl *et al.* 1951). The inflow branches of the Hadley circulation, also known as the trades, are filled with shallow cumulus clouds. These clouds increase the mixing of moist air away from the surface and drier free tropospheric air towards the surface. This increases the surface enthalpy flux, which is important for coupling the atmosphere to the ocean, and allows the trade-winds to accumulate plenty of heat and moisture as they travel equatorward.

When the European Center for Medium-range Weather Forecast (ECMWF) first introduced shallow convection in its model, increasing the ventilation of the boundary layer, the onset of deep convection was delayed, and the Intertropical Convergence Zone (ITCZ) narrowed (Tiedtke 1989). By changing the rate of ventilation by shallow convection, Neggers *et al.* (2007) found a similar effect in an intermediate-complexity quasi-equilibrium tropical circulation model (QTCM).

More recently, a number of studies show that the low-level cloudiness produced by shallow convection also narrows regions with deep convection. For instance, using a version of the QTCM, (Bretherton and Sobel 2002a) and (Peters and Bretherton 2005) show that

by adding cloud-radiative cooling to the top of the boundary layer the area occupied by deep convection in a Walker-like circulation is reduced. Cloud resolving model (CRM) simulations of the aggregation of deep convection reveal a similar mechanism. The areas with compensating subsidence that surround deep convection are relatively dry, and therefore experiences more low-level radiative cooling. Low-level clouds in the subsiding areas further enhance the cooling (Muller and Held 2012; Wing and Emanuel 2014; Hohenegger and Stevens 2016). In turn, this cooling triggers a circulation that aggregates moist static energy into the deep convective region, leading to further aggregation of deep convection, and an increase in the area with subsidence. Such mechanisms are critical for climate, because large areas with subsidence drying enhance the global emission of longwave radiation to space, leading to a global cooling (Pierrehumbert 1995; Nilsson and Emanuel 1999; Mauritsen and Stevens 2015).

Such studies suggest that vertical mixing and low-level cloudiness from shallow convection can have important large-scale effects. In fact, it might not come as a surprise that the same factors - vertical mixing and low-level cloudiness - help explain why climate models diverge in their prediction of climate sensitivity (Sherwood *et al.* 2014; Vial *et al.* 2016).

How shallow the convection is in the context of these studies is not entirely clear, but here we interpret it as cumulus humilis or mediocris with tops up to 2 km. Indeed, these low-level clouds dominate the trades. But we also know that episodes of these cumuli vary with episodes of deeper cumulus congestus, which have a much higher propensity to precipitate. Observations in the trades show that the time scale of this variability is on the order of a few days to a week (Nuijens *et al.* 2015), which suggests that they are tied to changes in the large-scale synoptic state, *e.g.*, atmospheric circulations.

What sets the depth of convection in the subsiding branches of circulations? Which interactions between the deep convecting and the subsiding areas, other than the relative area they occupy, can help explain the depth of convection and the distribution of precipitation within circulations?

In turn, the depth of (shallow) convection may influence the circulation. Large-Eddy Simulations (LES) show that the presence of congestus will produce deeper moist layers and smaller humidity lapse-rates, especially near the boundary layer top. This reduces the radiative cooling of the lower atmosphere (Vogel and Nuijens, *in preparation*). As suggested in the previously mentioned studies on the aggregation of deep convection, and demonstrated by Naumann *et al.* (2017), radiative cooling is just as important as gradients in sea-surface temperature (SST) in setting the strength of circulations. Furthermore, congestus introduces a latent heating to the atmosphere through precipitation. The relative importance of SST gradients and diabatic heating has in fact been a long-standing question in studies that seek to explain the distribution of tropical precipitation, and thus the intensity and width of the ITCZ. Most likely, both matter, as nicely reviewed by Sobel and Neelin (2006).

These questions and studies motivate the work we present here. We wish to understand what mechanisms are important for the depth of convection in the subsiding branches of a circulation at different SST gradients, and how the circulation adjusts with the properties of convection. Is congestus a stable mode in circulating equilibria of the tropical atmosphere? And how does the distribution of precipitation change with the character of the circulation?

Instead of a full-complexity climate model, in which interactions take place across so many scales they are hard to identify, we use a two-column equilibrium model, following a succession of studies that have used two- or four-box equilibrium models to understand the sensitivity of tropical climate (Pierrehumbert 1995; Sun and Liu 1996; Miller 1997; Clement and Seager 1999; Larson *et al.* 1999; Nilsson and Emanuel 1999; Bellon and Treut 2003). With the model, we can study fundamental aspects of the interaction of convection with a large-scale circulation, before turning to a cloud-resolving model with parameterized large-scale dynamics. The model we use numerically solves the hydrostatic equations of motion for non-rotating, non-linear flow in two side-by-side columns. A version of the model, but then for linear flow, was first used by Nilsson and Emanuel (1999). They demonstrated that the presence of a positive feedback between the circulation, clear-sky water vapour, and radiation can destabilise the radiative-convective equilibrium (RCE) state, which leads to a new equilibrium with a thermally direct circulation between the columns. A strong sensitivity of tropical circulations to water vapor, radiative cooling and cloudiness in the subsiding branch was also shown by others (Pierrehumbert 1995; Miller 1997; Larson *et al.* 1999).

In most two-column model studies, convection in the subsiding column is limited to the boundary layer, but in the present model the depth of convection is calculated interactively by the convection scheme. Radiation is also calculated interactively, and a cloud scheme is used. But we also make a number of important simplifications. We assume that the columns are of equal size, and for now neglect the important influence of the relative areal fractions of the convecting and subsiding branches on the circulation and climate (Pierrehumbert 1995; Bellon and Treut 2003; Mauritsen and Stevens 2015). We also prescribe the SSTs, knowing that surface winds and ocean transport play an important role at setting these (Sun and Liu 1996; Clement and Seager 1999). Furthermore, we ignore the interaction with mid-latitude synoptic systems, which are known to affect convection and cloudiness in the trades. For instance, cold air advected from higher latitudes is one of the better predictors of low-level cloudiness.

Despite these simplifications, and the fact that the parameterized physics carry similar uncertainties as the physics used in global climate models, the simplified geometry of the model allows us to get a first insight into mechanisms that are at play. In section 2 we describe the model physics and set up, and in section 3 we explain how the model evolves from a radiative-convective equilibrium state in both columns to a circulating equilibrium between the columns upon imposing a SST gradient. We will show that the model can produce a range of convective tops in the subsiding column that is independent of the vertical resolution, and which is reminiscent of the trimodality in convection in nature. We will describe the differences in the circulation and precipitation, depending on whether convection is deep, or collapses to a congestus or shallow mode. We find that the congestus mode is very sensitive to the details of the physics, including the moisture structure set by deep convection, the momentum of the flow, the interaction with radiation, and the efficiency of warm rain formation. The sensitivities are explained in section 4. We summarize our findings in section 5, and we also discuss which mechanisms might hold relevance to the real world, and which may be addressed in future modelling studies.

2. The model and experimental set up

2.1. Governing equations

The model is hydrostatic and based on the primitive equations for two-dimensional flow, which can be aligned in the zonal-height plane or meridional-height plane. The model has an ocean whose SST is prescribed in this study, and an atmosphere consisting of

Parameters control set-up		
Domain, resolution and integration		
vertical levels	N_z = 100	
domain length	L = 3000	km
integration time	T = 300	days
time step	Δt = 60	s
Surface fluxes and damping		
sea surface temperature	SST = 30	°C
gust factor	**V** = 7	ms^{-1}
surface transfer coefficient	C_D = 0.0015	
damping time scale	τ = 100	days
PBL depth	Δ_{PBL} = 150	hPa
Radiation		
latitude	ϕ = 10	°
time step for radiation calls	Δt_r = 60	s
solar constant	S = 1382	Wm^{-2}
ocean albedo	A = 0.15	-
Microphysics		
warm-cloud autoconversion threshold	l_0 = 1.1	gkg^{-1}
fraction of rainshaft falling through clear-sky	σ = 0.15	

Table 1. Parameters used in the control set-up of the two-column model and which are varied in this study. Optimized values for all parameters used in the convection (microphysics) scheme can be found in (Emanuel and Zivkovic-Rothman 1999).

two vertical columns, which can exchange heat through an overturning circulation. In the current set up we focus on (zonal mean) non-rotating meridional flow, which may be considered a mock-Walker circulation (Figure 1).

The model numerically solves the following equations for the temperature T, specific humidity q_v and the vorticity η:

$$\frac{\partial T}{\partial t} + u\frac{\partial T}{\partial x} + \omega\frac{\partial T}{\partial p} + \frac{\alpha\omega}{c_p} = \gamma\frac{\partial^2 T}{\partial x^2} + \frac{F_{\mathrm{SH}}}{c_p\Delta p} + Q_{\mathrm{R}} + F_{\mathrm{Q1}} \tag{1}$$

$$\frac{\partial q_v}{\partial t} + u\frac{\partial q_v}{\partial x} + \omega\frac{\partial q_v}{\partial p} = \gamma\frac{\partial^2 q_v}{\partial x^2} + \frac{F_{\mathrm{LH}}}{c_p\Delta p} + F_{\mathrm{Q2}} \tag{2}$$

$$\frac{\partial \eta}{\partial t} + u\frac{\partial \eta}{\partial x} + f\frac{\partial v}{\partial p} = \frac{\partial \alpha}{\partial x} + \gamma\frac{\partial^2 \eta}{\partial x^2} + \frac{\partial \nu(\partial\eta/\partial p)}{\partial p} + \frac{\partial F_c^u}{\partial p} \tag{3}$$

whereby the vorticity η of the flow is defined as:

$$\eta = \frac{\partial u}{\partial p} - \frac{\partial \omega}{\partial x} \tag{4}$$

and the specific volume α as:

$$\alpha = \frac{T\,R_d\,(1 - q_v + q_v/\epsilon)}{p} \tag{5}$$

Here, R_d is the gas constant for dry air, ϵ is the ratio of the molecular mass of water vapor and of dry air, u is the zonal wind and ω is the vertical velocity in pressure coordinates. In Equations 1 and 2, c_p is the specific heat capacity of dry air, and γ represents the inverse of a damping time scale τ, corresponding to the domain size L (see below). F_{SH} and F_{LH} are the sensible and latent heat fluxes at the surface, which are applied to the first model layer Δp; Q_{R} is the net radiative heating tendency; and F_{Q1} and F_{Q2} are the heat source and moisture source/sink due to convection and condensation. In Equation 3, f is the Coriolis parameter, which is put to zero in this study; F_c^u is the tendency of the zonal wind due to convective momentum transport; and $\frac{\partial \nu(\partial\eta/\partial p)}{\partial p}$ represents the momentum flux divergence in the boundary layer. ν is a shear viscosity, which is a function of pressure as follows:

$$\nu = \begin{cases} 100\gamma\left(1 + \frac{p - p_s}{\Delta_{\mathrm{PBL}}}\right), & \text{for } p \geq p_s - \Delta_{\mathrm{PBL}} \\ 0, & \text{for } p < p_s - \Delta_{\mathrm{PBL}} \end{cases} \tag{6}$$

The flow is thus non-linear, and forced by a zonal gradient in specific volume (α), which is inversely proportional to the virtual temperature. Enthalpy and moisture can be horizontally transported from one column to the other. The first terms on the right hand side represent a simple Fickian damping of the flow in the model interior through diffusion at a time scale τ. There is no obvious choice for what τ should be, and here we use $\tau = 100$ days for a domain size $L = 3000$ km (Table 1). In the boundary layer, the flow is damped through momentum flux divergence (Equation 6), which linearly decreases from a maximum damping near the surface to zero damping above the boundary layer, whose depth equals Δ_{PBL}. Additionally, momentum in the model interior is damped through convective momentum transport (see also section 2.2). A linearized surface-drag formula is used as the boundary condition at the surface, and a free-slip condition is used at the model top.

The two columns are of equal size and 1500 km wide. Each atmospheric column has $N_z = 100$ number of vertical pressure levels in the control set-up (Table 1), with the model bottom at p =1000 hPa and the model top at p =5 hPa. The vertical resolution is 12.5 hPa up to p =100 hPa, above which the grid is refined from 5 hPa up to 2.5 hPa.

The equations are solved using a leapfrog scheme in time with an Asselin filter and homogeneous Neumann boundary conditions. The model integration is performed using a time step of 1 minute and continued until equilibrium is reached, usually after 300 days for RCE, and 100 days for the circulating equilibria (Table 1).

2.2. *Parameterized physics*

The model uses parameterized convection, radiation and clouds to calculate the tendencies of heat, moisture and vorticity. The convection scheme is that of Emanuel and Zivkovic-Rothman (1999), and is particularly attractive for our study because the scheme does not explicitly distinguish between shallow and deep convection, allowing the transition between shallow and deep convection to be determined entirely by the model physics. The scheme computes undiluted updrafts, unsaturated downdrafts (see the formulation of precipitation below), and upward and downward mass fluxes that are based on the buoyancy sorting hypothesis of Raymond and Blyth (1986), which assumes that mixing is episodic and inhomogeneous. The scheme uses a spectrum of mixtures, which each ascend or descend to their level of neutral buoyancy. The fraction of the total cloud base mass flux that will mix with the environment at any given level is a function of the vertical change in undiluted cloud buoyancy. An increase in buoyancy with height leads to entrainment, and a decrease in buoyancy with height leads to detrainment. The mass flux at cloud base is derived by assuming that the sub-cloud layer remains neutrally buoyant with respect to air just above the sub-cloud layer. In other words, the cloud base mass flux responds to the difference between the virtual temperature of a parcel lifted adiabatically from the sub-cloud layer and the virtual temperature of the environment just above the sub-cloud layer. Instead of a separate boundary layer scheme, this model uses dry adiabatic adjustment below cloud base.

The scheme also computes the influence of convection on the zonal and meridional wind (convective momentum transport, CMT). Momentum is transported by the buoyancy-sorted updrafts and downdrafts just like a passive scalar, and conserves the mass-integrated momentum. A tunable factor multiplies the wind tendency and controls the strength of the CMT.

The formulation of microphysics in the convection scheme assumes that stochastic coalescence is the main precipitation forming process in warm clouds, and that the Bergeron-Findeisen process leads to more efficient precipitation formation when ice is involved. All cloud condensate beyond a critical threshold l_0 is removed from the updraft, whereby l_0 is constant below the freezing level and decreases linearly above the freezing level. No specific melting or freezing processes are included. Precipitation, once formed, does not interact with cloud water. It is added to a single hydrostatic, unsaturated downdraft, which transports heat and water, and which evaporates depending on the ambient temperature and humidity. This requires a number of parameters to be specified, for instance, the area fraction of the precipitation downdraft, or the fraction of the precipitation that falls through unsaturated air. We here rely on values for these parameters that are fine-tuned to observations made during GATE and TOGA COARE (Emanuel and Zivkovic-Rothman 1999). The specific parameters that are varied in this study are in Table 1.

The surface sensible and latent heat fluxes (F_{SH} and F_{LH}) are parameterized using standard bulk aerodynamic formulae:

$$F_{\mathrm{SH}} = \rho\, C_D |V_s| \,(\mathrm{SST} - T_1) \tag{7}$$

$$F_{\mathrm{LH}} = \rho\, C_D |V_s| \,(q_{s(\mathrm{SST})} - q_1) \tag{8}$$

using a surface transfer coefficient C_D that is the same for heat and moisture and the total absolute wind speed near the surface $|V_s|$. The latter is a function of the grid-box averaged surface wind speed, a gust factor $\mathbf{V}$, and a deep convective downdraft velocity scale (Emanuel and Zivkovic-Rothman 1999).

Longwave radiation is calculated using the scheme of Morcrette (1991) and shortwave radiation is calculated following Fouquart and Bonnell (1980). The shortwave radiation that we use is an annual averaged value for 10° latitude, and is not time- or date-dependent. Temperature, water vapor and clouds fully interact with radiation at every time step, but can be held static if desired, which we do in sensitivity tests in section 4.3.

Lastly, cloudiness is calculated using the statistical scheme of Bony and Emanuel (2001), which uses a probability distribution function of the total water, whose variance and skewness are diagnosed from the amount of sub-grid scale condensed water produced by cumulus convection, as well as from large-scale super-saturation. The scheme was originally optimized for tropical cumulus convection over the Pacific warm pool, and has been noted to underestimate low-level cloudiness. Especially near the lifting condensation level or cloud base, values for cloud fraction are small. Therefore, we interpret low-level cloudiness and its radiative effect with some caution. Because studies have suggested that radiative effects from low cloud may play an important role in driving circulations Bretherton and Sobel (2002b); Muller and Held (2012) this aspect certainly deserves more attention. But in this study we accept this shortcoming (along with others) and focus on understanding the mechanisms behind sensitivities to the physics, regardless of their imperfections.

3. From radiative-convective equilibrium to circulating equilibria

3.1. *Local RCE*

Before imposing a SST difference, the radiative-convective equilibrium (RCE) state is calculated and applied to both columns (Figure 1a). The mean sounding of the TOGA COARE field campaign is used to initialise the model, but technically, any sounding can be used, because the model physics control the final thermodynamic state. The model is forced with a SST of 30°C, and the annual and daily averaged solar insolation at a 10° latitude (Table 1). The model is run at three different vertical resolutions (Δp =25, 12.5 and 6 hPa), whose corresponding RCE states are plotted in Figure 2.

In RCE, convection has an upward mass flux that is positive up to 150 hPa (Figure 2a). This produces a convective heating that balances the radiative cooling rate of the atmosphere (Figures 2c and d). Precipitation produces unsaturated downward mass fluxes at and below 300 hPa (Figure 2b), and surface precipitation rates average to 5 mmd^{-1}. Cloudiness peaks in the upper atmosphere where the atmosphere is close to saturation, and is small at low-levels (Figures 2e and f).

The sensitivity of the model to vertical resolution is small, except for the sharpness of moisture inversions, which slightly increases with resolution. For instance, see the inversions at the top of the mixed layer at 950 hPa or at 350 hPa (Figure 2e). This also results in stronger peaks in radiative cooling (Figure 2d). We will further discuss this particular moisture structure in RCE in section 3.4.

Because both columns have an identical RCE state, no horizontal gradients in specific volume are present. Therefore, there is no horizontal flow between the two columns and the vertical velocity in each column is zero. For some combination of physical parameters an oscillation between the columns can develop, as one column develops larger high-level cloudiness than the other column at individual

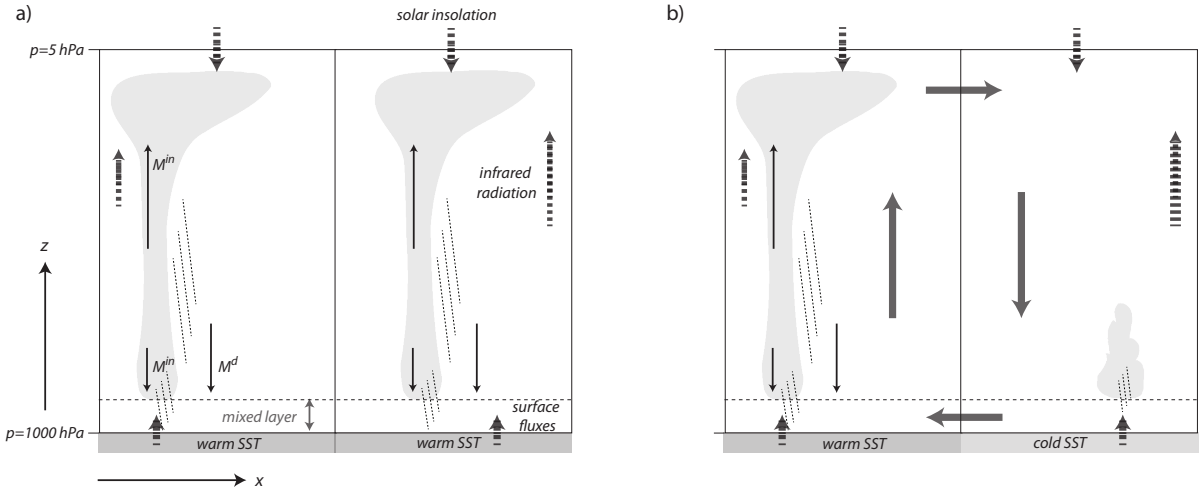

Figure 1. A schematic of the two-column model framework. a) The two columns supporting deep convection over warm SSTs, whereby each column is in local radiative-convective equilibrium. b) The SST of the rightmost column has been lowered, and convection over the colder ocean has collapsed. A circulating equilibrium between the two columns has been established, with mean ascent over the warm ocean and mean descent over the cold ocean.

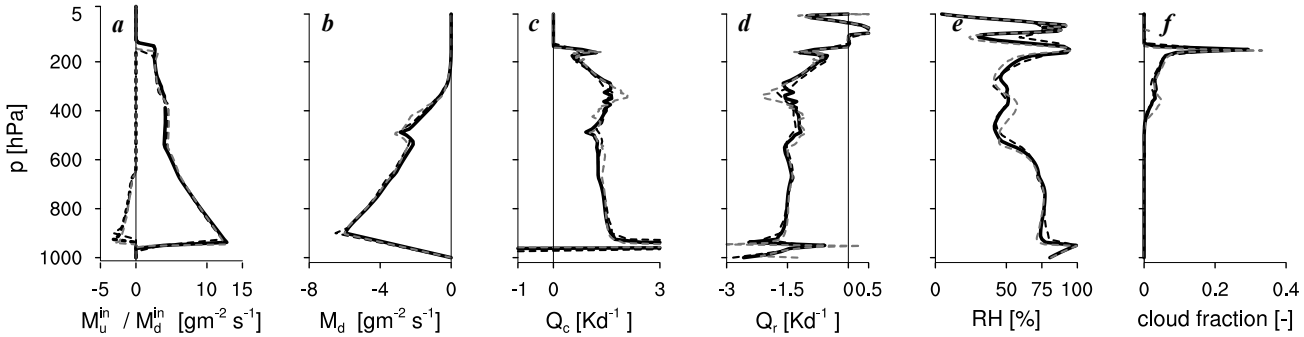

Figure 2. Profiles of the local radiative-convective equilibrium state of the columns at SST = 30°C for different vertical resolutions: Δp =12.5 hPa (control case - solid black line), Δp =25 hPa (dashed black line) and Δp =6 hPa (dashed grey line). The following variables are shown: a) the saturated upward mass flux $M_u^{\rm in}$ and downward mass flux $M_d^{\rm in}$; b) the unsaturated precipitation-driven downward mass flux M_d; c) the convective heating rate Q_c; d) the radiative cooling rate Q_r; e) the relative humidity RH; and f) the cloud fraction.

time steps, which causes different radiative heating rates. Weak horizontal and vertical flows then develop, which continuously reverse. When radiation is not called every time step, these differences in radiative heating rates can persist for longer periods of time, and lead to the collapse of convection in one column, whereas convection in the other column remains deep (Pauluis and Emanuel 2004). Here we avoid this form of spontaneous aggregation by calling radiation every time step.

3.2. *A thermally-forced circulation*

After the RCE state is applied to both column, a thermally direct circulation is forced by lowering the SST in one of the columns by increments of 0.25K. Alternatively, the SST may be raised from a colder RCE state, but this atmosphere in that state will be less humid. The circulations that develop are sensitive to the initial moisture structure, and therefore, there is some hysteresis between runs that start out at different SSTs. But the hysteresis is not large enough to change the overall character of the circulation that develops, and we only show results of runs starting from a warm RCE state.

Over the colder sea surface convection collapses, and the absence of deep convection cools the upper troposphere. This creates a heating contrast with the other column where convection is still deep, and therefore, upper level winds will develop that are directed from the warm to the cold column, along with a sinking motion over the cold ocean (Figure 1b). The strength of the subsidence in this column depends strongly on how the thermodynamic and cloud structure evolve with the circulation, because these will control the radiative cooling profile . As first described by (Nilsson and Emanuel 1999), the drying that results from subsidence will further enhance the emission of infrared radiation from the moister layers underneath, and therefore lead to more low-level cooling: a positive feedback. Without this feedback the subsiding column can still develop deep convection for SST differences less than 1.5K, as we will show in section 4.3 (*e.g.,* Figure 10).

In our runs a new circulating equilibrium develops within 100 days, usually already after 30 days. RCE has then been replaced by a balance between (shallow) convective heating, radiative cooling and subsidence warming over the cold ocean, and (deep) convective heating, radiative cooling and adiabatic cooling over the warm ocean. Profiles of the thermodynamic and mass flux structure in the columns for different Δ SST are shown in Figure 3, and profiles of the circulation (vertical and horizontal winds) and the convective heating and radiative cooling profiles are shown in Figure 4. All results are for the control set-up with a vertical resolution of N = 100 and Δp =12.5 hPa.

Upon gradually decreasing the SST, convection in the cooled column collapses, but the collapse is step-wise. For small SST differences (ΔSST$<$ 0.5K) convection over the cold ocean remains deep with stable convective tops near 150 hPa (brown-hued profiles

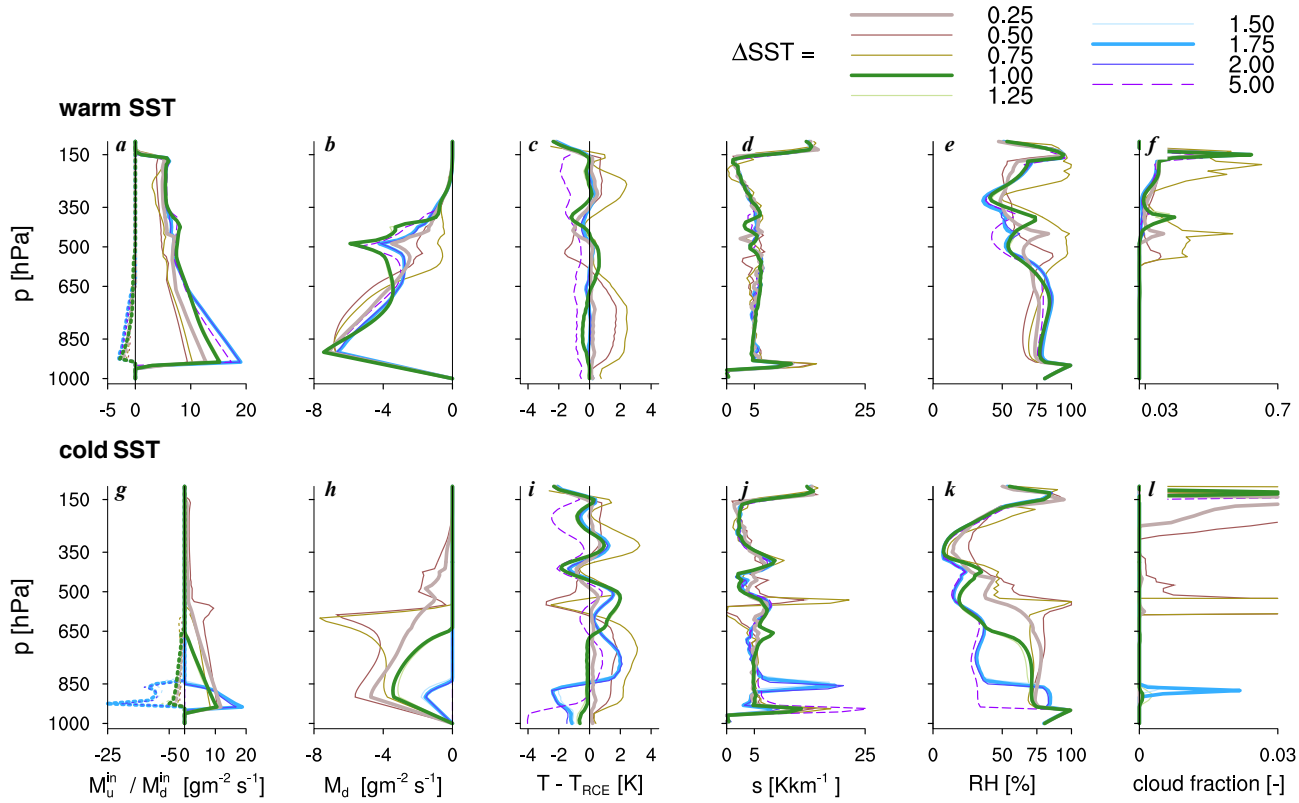

Figure 3. The mass flux, thermodynamic and cloud vertical structure in the warm SST (top panels) and cold SST column (bottom panels) as a function of ΔSST. Plotted are: a,g) the saturated (in-cloud) upward mass flux (M_u^{in}) and downward mass flux (M_d^{in}); b,h) the unsaturated out-of-cloud downward mass flux (M_d); c,i) the temperature minus the initial temperature in the RCE state; d,j) the static stability S; e,k) the relative humidity RH; and f,l) the cloud fraction.

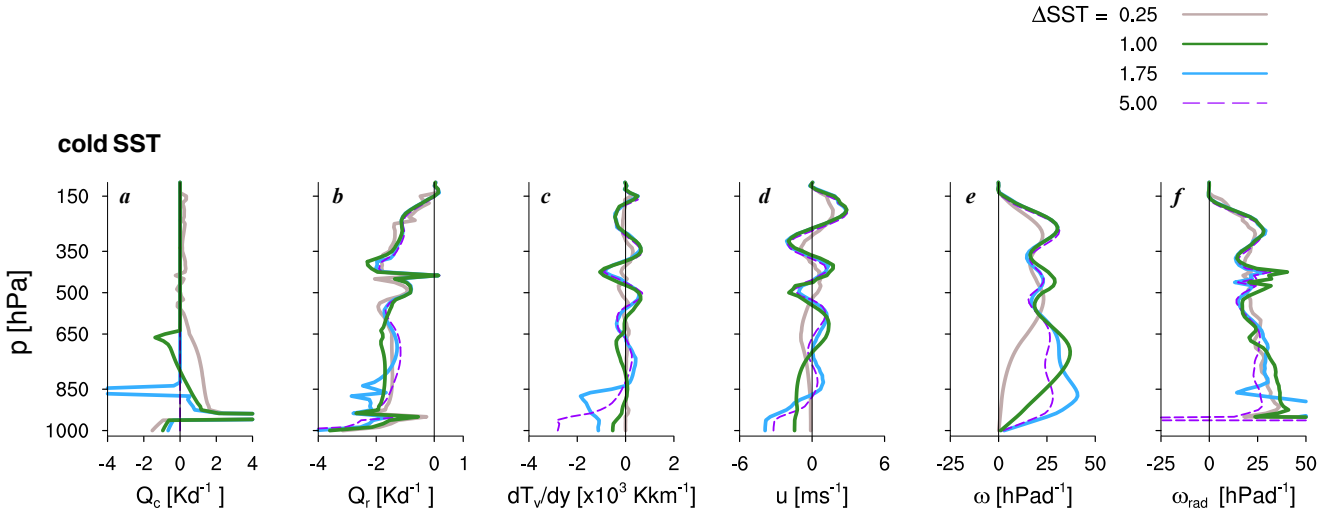

Figure 4. Profiles of the structure of the circulation and the convective and radiative heating tendencies over the cold SST column. Plotted are: a) the heating tendencies due to convection Q_c; b) the radiative cooling profile Q_r; c) the virtual temperature (buoyancy) gradient between the two columns dT_v/dy; d) the horizontal velocity u at the column boundary; e) the vertical velocity over the cold ocean ω^{cold}; f) the radiative vertical velocity $\omega_{\text{rad}}^{\text{cold}}$ (see text for further explanation).

in Figure 3g), but much less mass flux penetrates to 150 hPa, as compared to the deep convection over the warm ocean (Figure 3a). When ΔSST = 1K (green-hued profiles) convection drops down preferably to the 550 hPa level (≈ 0°C) and the 650 hPa level, whereas when ΔSST> 1.5K (blue-hued profiles) convection drops to 875 hPa. The same result is plotted in Figure 5a by means of the convective top, defined as the maximum level of positive convective mass flux, as a function of ΔSST. The colours correspond to the colours of the profiles in Figure 3 and 4. The squares denote the mean convective top over the last 30 days of model integration, and vertical bars through the squares denote the minimum to maximum convective top during those 30 days. The latter gives an indication of how stable the modes are, and reveals that convection at ΔSST = 1 K and 3-4 K tends to be less stable. At ΔSST > 2K, convection becomes very shallow, and approaches what may be thought of as a stratocumulus regime. But in the absence of convection, the model physics (*e.g.*, the absence of a separate boundary layer scheme) are no longer appropriate, and the results should not be over-interpreted.

We used SST increments even smaller than 0.25K (not shown) to confirm that the collapse of convective tops is indeed step-wise. The convective tops near 150 hPa, 650-550 hPa and 875 hPa bring to mind the observed trimodality of convection in tropical atmospheres, resembling deep cumulus convection, cumulus congestus and shallow cumulus convection (Johnson *et al.* 1999). The tendency of the model to produce congestus, or even oscillatory modes in between shallow and congestus, is intriguing. Namely, the model's

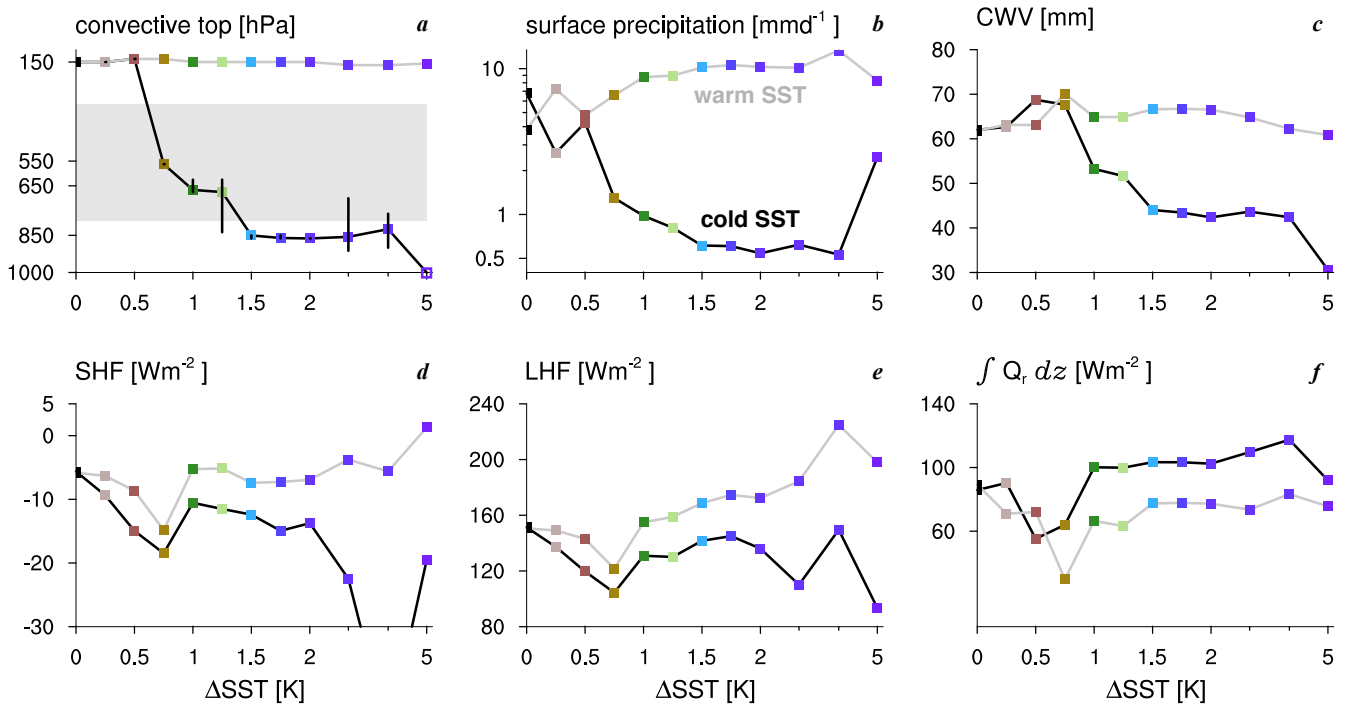

Figure 5. a) Convective tops as a function of the SST gradient (ΔSST), with black lines for the cold SST column and grey lines for the warm SST column. Convective tops are defined as the maximum level of positive in-cloud mass flux. When no mass flux is present, the convective top is put at 1000 hPa. Unstable tops are denoted with a vertical bar, which stretches from the minimum and maximum top that is attained in the last 30 days of model integration. The gray shading indicates congestus tops between roughly 2 - 8 km. Other variables shown are: b) the surface precipitation rate, c) the column water vapor, d) the sensible heat flux, e) the latent heat flux and f) the radiative cooling rate integrated from the surface up to 500 hPa.

microphysics scheme does not include explicit freezing or melting, which is believed to play an important role at halting congestus at mid-levels. Because the vertical grid spacing (Δp = 12.5 hPa) is much smaller than the distance between the preferred levels of convection, the model physics must be responsible for these modes (section 3.4).

As the convection shallows, the upper and middle atmosphere dries, and the moisture gradient at the top of the convective layer strengthens (Figure 3k). A stable layer near 950 hPa (cloud base) is visible in the profile of RH and the static stability, defined as $s = d\theta/dz$ (Figure 3j). This stable layer is a robust feature of the convection scheme and can be interpreted as the top of the well-mixed sub-cloud layer, which helps regulate the mass flux at cloud base. Over the cold ocean, a second stable layer can be found near the tops of convection, where detrainment takes place and cloudiness peaks (Figure 3l). At this inversion, convection produces a cooling instead of a heating due to the strong mixing and evaporation of condensate (Figure 4a). The radiative cooling profile over the cold ocean responds strongly to the RH structure that develops (Figure 4b). The shallow modes with stronger moisture gradients near the inversion cool more strongly below 850 hPa than the congestus modes. The latter instead occur along with a more humid layer between 800-650 hPa, which cools more radiatively, but reduces radiative cooling of layers underneath.

The circulation is strong where the heating contrast between the columns is large. When deep convection over the cold ocean has collapsed, for ΔSST $>$ 0.5K, the heating contrast maximizes near the tops of the cold-side convection. This is where radiative and evaporative cooling peak. Hence, horizontal flows from the warm to the cold column are strongest near the tops of respectively the shallow and congestus modes (Figure 4c). This is also where subsidence peaks (Figure 4d). The horizontal return flow (or "shallow" return flow, as it is often called in the literature) illustrates that overturning circulations are not necessarily deep overturning circulations. In fact, shallow overturning circulations have been observed on the scale of the Hadley and Walker circulations, in different ocean basins and in different seasons (Zhang *et al.* 2008). In our runs, the horizontal wind reverses twice more above 650 hPa. This structure, which corresponds to persistent horizontal buoyancy gradients at those height levels, is discussed in section 4.2.

Because we use only two columns, mass conservation dictates that mean ascent in the warm column equals descent over the cold ocean: $\omega^{\text{warm}} = -\omega^{\text{cold}}$. As such, profiles if ω^{warm} are not separately shown. As we described above, ω^{cold} and horizontal winds respond to heating contrasts. Over the cold ocean, the diabatic heating above the tops of convection consists only of radiative cooling. The radiative vertical velocity ($\omega^{\text{cold}}_{\text{rad}}$), which is the vertical velocity required to balance the radiative cooling Q_r (Figure 4b) divided by the profile of stability (Figures 3d,j) closely follows that of ω^{cold} above convective tops (Figure 4f). However, below convective tops, the heating or cooling from convection is large enough to either counteract or reinforce (radiative) cooling, and thus becomes a significant term in explaining the profile of low-level winds.

This implies that when evaporative and radiative cooling over the cold ocean are not that pronounced, the circulation is not that strong. This can be true even at larger ΔSSTs, which is illustrated by the run with ΔSST = 5K (dashed purple line in Figures 3 and 4). At that ΔSST convection has completely collapsed, which results in a very dry free troposphere above a mixed-layer layer, which is capped by a strong inversion (Figures 3 h and i). No more cloud is present near the mixed-layer top (Figure 3l). Both the dryness and the lack of cloudiness reduce the radiative cooling between 950 and 650 hPa (Figure 4b). As a result, the circulation, as measured by near-surface winds (Figure 4d) and low-level subsidence (Figure 4e), is even weaker than in the run with ΔSST = 1.75 K.

3.3. *Response of the warm column*

The increasing ΔSST and collapse of convection over the cold ocean do not affect the depth of the convection over the warm ocean, where convective tops remain near 150 hPa (Figures 3a and 5a). But the upward mass flux at cloud base approximately doubles

from ΔSST = 0.25 K to ΔSST = 1.75 K. Some of that larger cloud-base mass flux goes into larger detrainment below mid-levels, corresponding to larger relative humidities up to 650 hPa (Figure 3e). In the model's convection scheme, the cloud-base mass flux is relaxed toward sub-cloud layer quasi-equilibrium. That is, the scheme adjusts the cloud-base mass flux in response to the difference between the density temperature of a parcel lifted from the sub-cloud layer and that of the environment near the lifting condensation level. If the sub-cloud layer warms relative to the lower cloud layer, the lower atmosphere is more unstable with respect to rising parcels, and the mass flux will increase.

Indeed, the runs with a shallow mode in the descending column (blue-hued profiles) have a relatively warm sub-cloud layer and unstable lower atmosphere, and therefore a relatively large cloud-base mass flux, as compared to runs with congestus or deep modes. This can be seen from the temperature anomaly profiles over the cold ocean (Figure 3i, whereby the anomalies are taken with respect to the same initial temperature profile in RCE). It is also true for the warm column, although much smaller there (Figure 3c). The decrease in stability near cloud base as convection over the cold ocean shallows is also seen in the static stability (Figure 3d and j), and is related to larger radiative cooling near and above cloud base (*e.g.*, Figures 4b). The deeper modes (brown-hued) instead have a larger stability due to less radiative cooling below 800 hPa, which is caused by a more humid lower and middle atmosphere or by large cloud fraction at mid-levels. Large mid-level cloudiness is produced by some of the deeper modes over both the cold and warm ocean, Figures 3f and l, and leads to relatively large radiative cooling rates compared to having the same amount of cloud at high-levels (not shown).

In summary, as the strength of the circulation increases with a collapse of convection over the cold ocean, the cloud-base mass flux over the warm ocean increases. The enhanced drying of the sub-cloud layer (along with stronger surface winds) lead to larger surface evaporation and larger precipitation rates over the warm ocean (Figures 5b and e). Thus, consistent with studies cited in section 1, more low-level radiative cooling, produced by more low-level cloud amount or moist boundary layers underneath dry free troposphereres, can increase the strength of the circulation and lead to changes in the character of deep convection. Here, this means an increase in surface precipitation rates. But at moderate ΔSSTs convection in the subsiding branch does not collapse to a shallow mode. Instead, a congestus mode develops, which has less low-level radiative cooling, and hence, a weaker shallow overturning circulation and less deep convective precipitation over the warm ocean.

In the next section we will discuss the ability of the model to produce trimodal convection. In fact, the model can produce a range of convective tops between shallow and congestus. Although multiple modes appear to exist, we still characterize the convection as trimodal.

3.4. Trimodality in convection

To understand why the model produces a trimodality in convection, we return to the RCE runs. Already in RCE the convection scheme detrains moisture at preferable levels, which are near cloud base, near the freezing level, and near 150 hPa. As we will explain below, these physics help create a moisture profile with a relatively dry layer above the freezing level. When a circulation develops, this dry layer will help limit congestus modes over the cold ocean by the formation of a stable layer, which develops through the interaction with radiation.

In nature, dry layers in the atmosphere are common, and have been observed along with stable layers near their base (Mapes and Zuidema 1996; Pakula and Stephens 2009). Congestus tops, but also detrained cloud layers that accompany deep convection, are often observed near the freezing level, and are also sometimes accompanied by stable layers (Johnson *et al.* 1999; Luo *et al.* 2009). Cloud-resolving simulations of tropical atmospheres also produce a peak in convective tops and a stable layer near the freezing level (Posselt *et al.* 2008; Mechem and Oberthaler 2013)). A stable layers near the freezing level is thought to arise from melting and freezing processes, in particular, from the melting of stratiform rain, which can produce a cooling below the freezing level. Once melting of ice has formed a stable layer, it may remain present after convection has decayed, or exchanged with the surrounding environment through gravity waves. In doing so it may limit subsequent or nearby convection.

In our convection scheme, there is no explicit freezing or melting, although a number of cloud physics parameters change values across the freezing level to represent liquid or ice. In a number of RCE runs with increasing idealisation (Figure 6) we explore the origin of preferred modes of convection in our model, and show that microphysics are not responsible for the trimodality. In these idealised runs we use clear-sky radiation to make sure that changes in radiative cooling caused by thermodynamics are not overshadowed by those related to excessive cloudiness, which develops when we turn off precipitation.

In a first test, we keep microphysical parameters constant across the freezing level (Figure 6, **1. microconstant**). Among these are the liquid water threshold for rain formation, l_0 (section 2.2), and the evaporation rate and fall speed of precipitation (Emanuel and Zivkovic-Rothman 1999). The RCE state from Figure 2 is plotted here in grey, and besides the saturated mass flux, radiative cooling, convective heating and relative humidity, we also plot the static stability s and the specific humidity q. The constant microphysics run is overall very similar to the control run, except that a stable layer near 550 hPa is now even more pronounced (Figure 6 - 1e). Additionally, the layer above 350 hPa is saturated, because of less precipitation above the freezing level (l_0 is constant with height instead of decreasing with height), and the layer between 550-350 hPa is drier (Figure 6 - 1d), because there is also less precipitation to evaporate.

The mass flux profiles of the control and constant microphysics runs (Figure 2a) have a discontinuity near the freezing level, with a near constant mass flux profile above the freezing level. The latter implies little detrainment above the freezing level, which explains why this layer is relatively dry. The structure of detrainment becomes even more pronounced when we remove condensate from the parcel updraft immediately, by setting the condensate-to-rain threshold l_0 to 0. This implies that condensate no longer plays a role in setting the mixture's detrainment levels. Additionally, we do not let any of that precipitation evaporate on its way to the surface (Figure 6 **2. noprecipevap**). Without evaporation of precipitation, the lower atmosphere is much drier, and any moistening is solely caused by detrainment. The preference of convection to detrain moisture near 650-550 hPa is now even more pronounced (Figure 6 2-d and 2-f). The strong moisture gradient at mid-levels leads to a peak in radiative cooling and enhanced stability at mid-levels (Figure 6 2-c and 2-e), similar to what previous studies have described (Mapes and Zuidema 1996) and (Pakula and Stephens 2009).

To demonstrate that the interaction of radiation with the humidity structure underlies the enhanced stability, the radiation calculations in test **3. radmoistoff** use a linear water vapor profile that is constant in time. With only the interaction of temperature with radiation, the radiative cooling no longer peaks at mid-levels, but has a minimum there instead. Yet, detrainment near mid-levels is still pronounced.

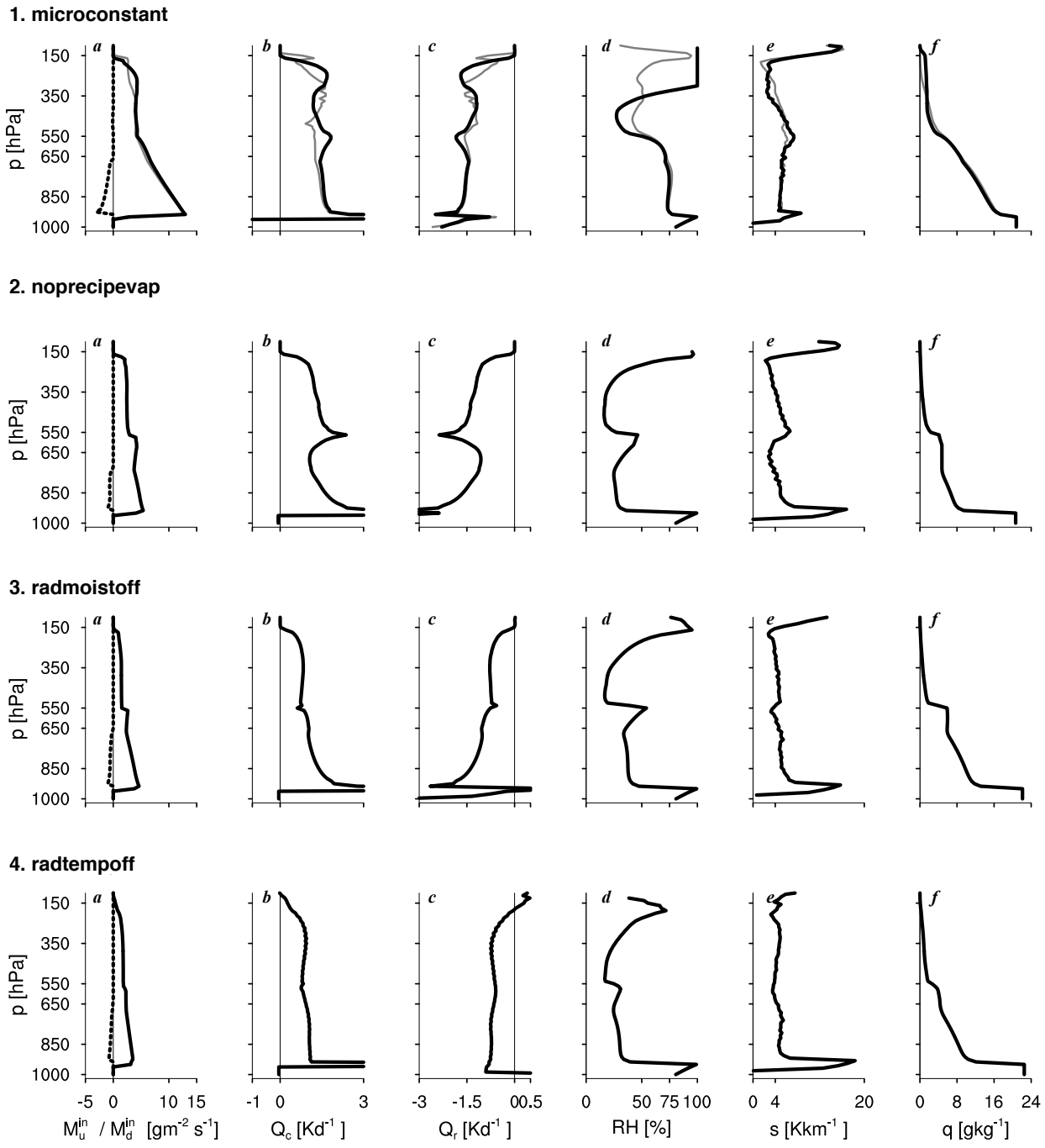

Figure 6. Profiles of the RCE state of the columns at SST = 30°C (*e.g.*, Figure 1a.) for a set of runs with increasing simplifications (see text for details): **1. microconstant**, microphysical parameters are constant across the freezing level and clear-sky radiation is used; **2. noprecipevap**, all liquid is immediately removed via precipitation (l_0 =0 gkg^{-1}) and there is no evaporation of precipitation; **3. radmoistoff**, in addition, there is no interaction between radiation and moisture; **4. radtempoff**, in addition, there is no interaction between radiation and temperature. The control set up from Figure 2) is shown in grey in the top panels. Variables plotted are: a) the saturated upward mass flux M_u^{in} and downward mass flux M_d^{in}; b) the convective heating rate Q_c; c) the radiative cooling rate Q_r; d) the relative humidity; e) the static stability s and f) the specific humidity q.

In a final step we also remove the interaction of radiation with temperature by using the initial TOGA COARE temperature profile for radiation calculations. This profile does not have pronounced stable layers, and therefore the radiative cooling profile is much more smooth (Figure 6c, **4. radtempoff**). But even in this run the convection scheme prefers detrainment at mid-levels, as indicated by the mass flux and humidity profiles in Figure 6c. In more detail, Figure 7 shows profiles of detrained and entrained mass fluxes for a number of representative time steps during the first thirty days of **4. radtempoff**. The convection scheme produces a set of undiluted updrafts, from which a spectrum of mixtures is calculated, which ascend or descend to the levels at which their liquid water moist static energy equals that of their environment. Panel a of Figure 7 reveals at what levels those mixtures are detrained, and shows that detrainment is large near cloud base, near the freezing level and near the tropopause. Panels (b-d) show from which levels those detrained mixtures originate, illustrating that air detraining at low levels is coming down in downdrafts that have resulted from mixing, while at higher levels the entrained air comes from below the detrainment level.

Hence, already in RCE, convection has a preference for a third middle mode, which appears unrelated to precipitation, or other discontinuities across the freezing level (*e.g.*, the saturation vapor pressure), which we removed in additional tests (not shown). This suggests that detrainment at mid-levels is fundamental, rather than an artefact of the scheme, which is corroborated by the fact that

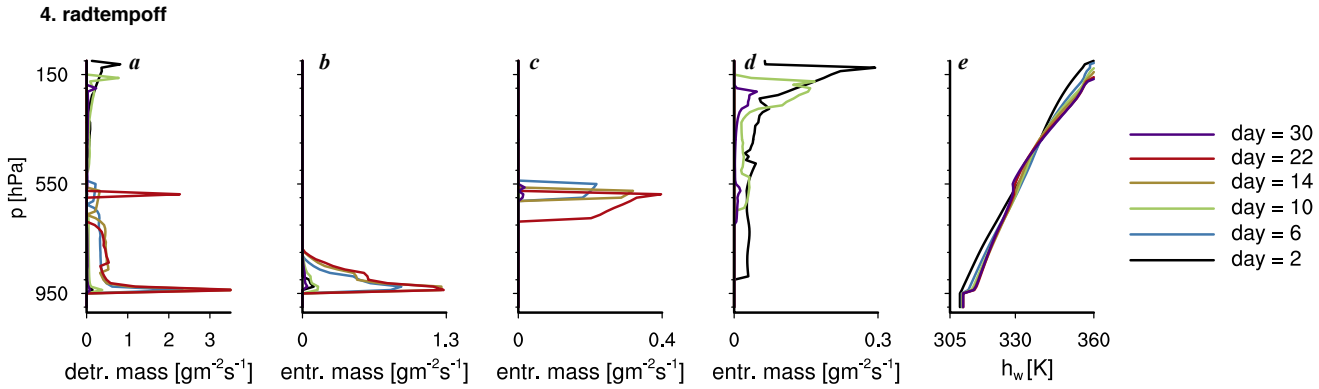

Figure 7. Instantaneous profiles of the detrained and entrained mass flux of mixtures plotted every few days for sensitivity test **4. radtempoff**) in Figure 6. Plotted are: a) the distribution of net detrained mass at each level, b) the distribution of entrained mass that is detrained at levels J = 950-900 hPa, c) same as in b) but for levels J = 600-550 hPa, d) same as in b) but for levels J = 200-100, e) the liquid water static energy h_w.

detrainment does not happen exactly at 550 hPa, but at a number of levels between 575-537 hPa. The most probable explanation for detrainment at mid-levels is the relative minimum in radiative cooling there, which appears to be typical for a tropical temperature profile, with high temperatures near the surface and near the tropopause (Figure 6-5c). From the very start of run **4. radtempoff**, the level of neutral buoyancy is indeed often at mid-levels, alternating with high-levels. The convection scheme is designed such that air is detrained at the same liquid water static energy as the environment. Theoretically, this cannot change the temperature of the environment. But the exception is the level of neutral buoyancy, since neutral buoyancy is not the same as equal liquid water static energy. Hence, cumulus tops near the freezing level are cooling the environment, which h_w illustrates (Figure 6e). Lapse rates above 0°C can even become superadiabatic, so that subsequent parcels crossing the freezing level can continue all the way towards the tropopause.

The trimodality of convection in this model is thus a result of how the model establishes RCE. The tests, as idealised as they are, illustrate the complexity of RCE, and suggest that melting of ice is not the only process that may create trimodality in nature. In the next section we will look into more detail at how the thermodynamic structure set in RCE leads to specific shallow and congestus tops in the circulations that develop, and show the sensitivity of these results to the model's vertical resolution, domain size, and other physics.

4. Sensitivity to model set-up and physics

Mixing processes in the convection scheme are expected to be sensitive to vertical resolution. Furthermore, although the imposed SST gradient plays a large role in setting the strength of the circulation, the gradient itself is a function of the model's domain size. An important question is thus how the vertical and horizontal resolution (domain size) influence the depth of convection that develops over the cold ocean. In section 4.2 we further discuss how momentum diffusion plays an important role at setting the specific tops of the shallow mode, and also helps the congestus mode to develop. Finally, the role of interactive radiation and warm rain in setting the specific tops of congestus is explained in section 4.3.

4.1. Vertical resolution and domain size

The convective tops of three runs at different resolutions are plotted in Figure 8a. The control run is plotted in solid black (a copy from Figure 5), along with runs at a lower vertical resolution (N_z = 46 and Δz = 250 m, black dashed line) and at a higher vertical resolution (N_z = 200 and Δz = 60 m, black dot-dashed line). At a lower vertical resolution deep convection collapses at slightly larger ΔSSTs, and after passing through one congestus mode at ΔSST = 1K, shallow modes remain. At a higher vertical resolution deep convection instead collapses at smaller ΔSST's, but a few congestus modes remain, before convection collapses to shallow modes. Hence, across all resolutions we observe a trimodality, which is inherent to the model physics (section 3.4).

For ΔSST $>$ 2 K the runs diverge. In this regime the simulated cloud amount at the top of the boundary layer, which starts to approach a stratocumulus regime, is very sensitive to the vertical resolution. At a higher vertical resolution more cloudiness develops, which results in more low-level radiative cooling (not shown). This cooling helps destabilize low-levels and maintains convection to some extent, in contrast to a lower vertical resolution, at which convection and cloudiness completely disappear.

The horizontal domain size can influence the results in a number of ways. First, the SST gradient between the columns increases with a decreasing domain size, and so will the horizontal gradients in buoyancy (or α), vorticity, meridional wind, temperature and humidity (Equations 3-2). A smaller domain should thus strengthen the circulation as measured by the vorticity, and strengthen horizontal advection. Second, the model damps momentum, temperature and humidity in the model interior as a function of their horizontal gradients (and the damping time scale τ). This acts like a diffusion, which will be more efficient for a smaller domain.

Figure 8b shows how convective tops change using a smaller domain (L = 500 km, black dot-dashed line) and a larger domain (L = 6000 km, black dashed line), while keeping τ unchanged. On the smaller ($L = 500$ km) domain deep convection collapses immediately to shallow convection, whereas the larger domain maintain a congestus mode. Larger domains also allow for deeper shallow modes, and overall, convective tops decrease more gradually as ΔSST increases.

The profiles of the buoyancy gradient (dT_v/dx) and the circulation as measured by u and ω help us understand this behaviour (Figure 9, top and middle panels). The gradients of the $L = 500$ km run in this Figure ($1/dx$) have been scaled (reduced by a factor of six) to compare with the control run, which uses $L = 3000$ km. Figure 9f thus shows that (after scaling) the gradients in T_v are relatively small for $L = 500$ km run compared to the control run (Figure 9a), especially above 900-850 hPa. Temperature gradients above those levels,

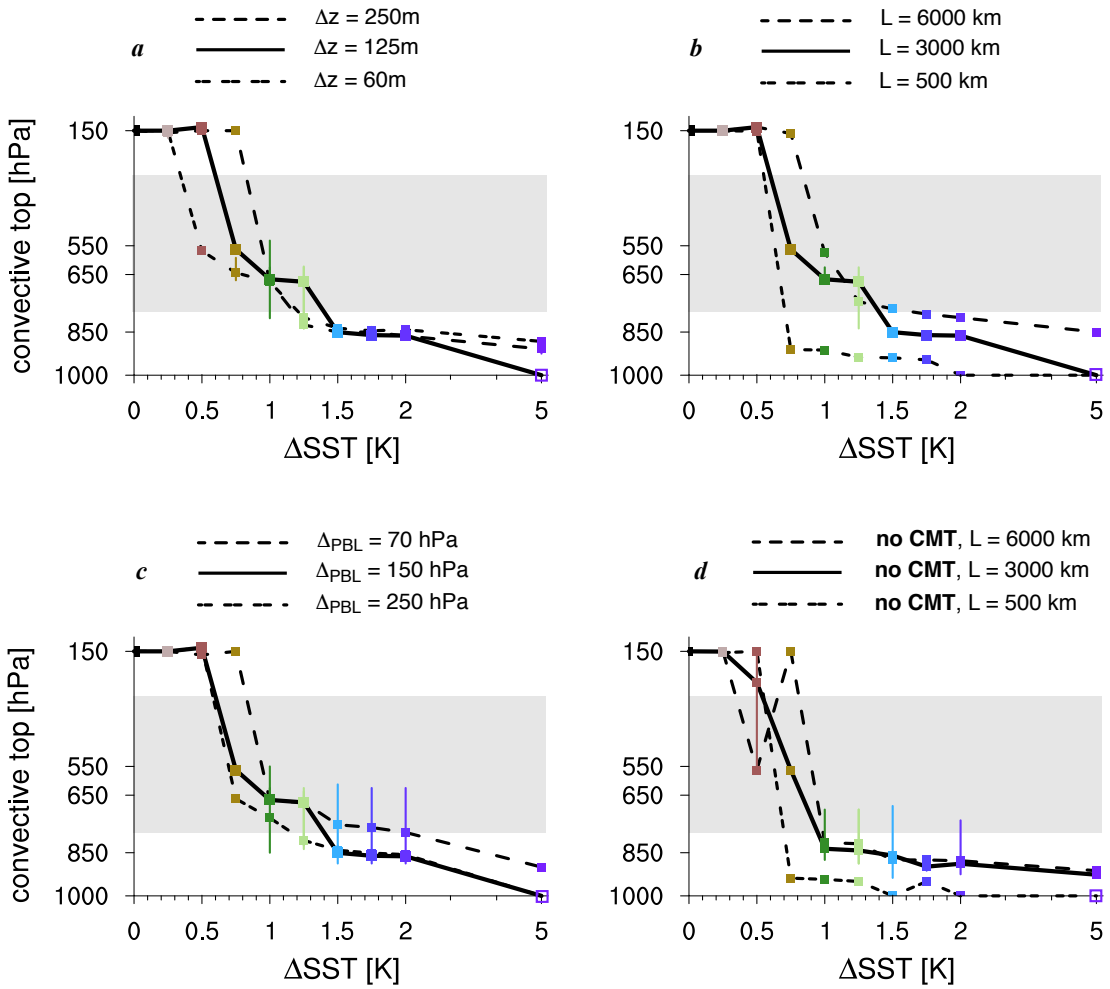

Figure 8. Convective tops over the cold ocean as a function of ΔSST as in Figure 5a), but here for a) different vertical resolutions including Δz = 60 m, 125 m (control) and 250 m; b) for different horizontal domain sizes, including L = 6000 km, 3000 km (control) and 500 km; c) for different PBL depths for momentum flux convergence, including Δ_{PBL} = 70 hPa, 150 hPa (control) and 250 hPa; and d) for different horizontal domain sizes, but without applying CMT.

for instance, those created by stronger evaporative or radiative cooling from congestus tops, are apparently difficult to maintain as buoyancy waves and damping become more effective at removing them. In other words, the weak virtual temperature gradient (WTG) approximation applies much better for small domains.

Without scaling, the gradients in T_v in the boundary layer are of course much larger for the $L = 500$ km domain. Therefore, the shallow and congestus modes (in blue and green) have a stronger circulation, which is marked by the larger maximum in subsidence near convective tops over the cold ocean, and accordingly, a larger maximum in ascending motion in the warm column (not shown). The near-surface wind speed at the column boundary is nevertheless smaller, because the two-column system requires mass continuity:

$$u = -\int \left(\frac{d\omega}{dp}\right) dx \tag{9}$$

whereby a larger $d\omega/dp$ is easily outweighed by a six times smaller dx.

A more accurate approach would be to reduce the damping time scale τ (Table 1) along with reducing the domain size. If τ is reduced for the $L = 500$ km domain, the damping applied to the model interior is even stronger. Using a six times smaller τ (not shown) we find that temperature and humidity gradients between the columns get smaller, but the results are otherwise similar, with similar convective tops. Hence, the influence of domain size is exerted mostly through setting buoyancy gradients and advective tendencies, and less so through damping.

However, the damping of momentum does play an important role, namely, in allowing buoyancy gradients to persist against the work of buoyancy waves, which we discuss next.

4.2. *Diffusion of momentum and stability of convective tops*

The explicit damping of momentum in the model interior as a function of τ, discussed in the previous section, is a relatively small term compared to other mechanisms through which the model diffuses momentum. One mechanism is the transport of momentum by the buoyancy-sorted updrafts and downdrafts (convective momentum transport, CMT), which is represented by F_c^u in Equation 3. Additionally, turbulent mixing in the boundary layer produces a vertical diffusion of momentum, which in the model is represented through the term $\frac{\partial \nu(\partial \eta/\partial p)}{\partial p}$ in the same equations, whereby ν depends on the damping time scale ($\gamma \propto 1/\tau$) and the boundary layer depth (Δ_{PBL}). Both processes have a similar effect on the results: they damp buoyancy waves that tend to smooth virtual temperature gradients. In doing so they allow buoyancy gradients between the columns to persist.

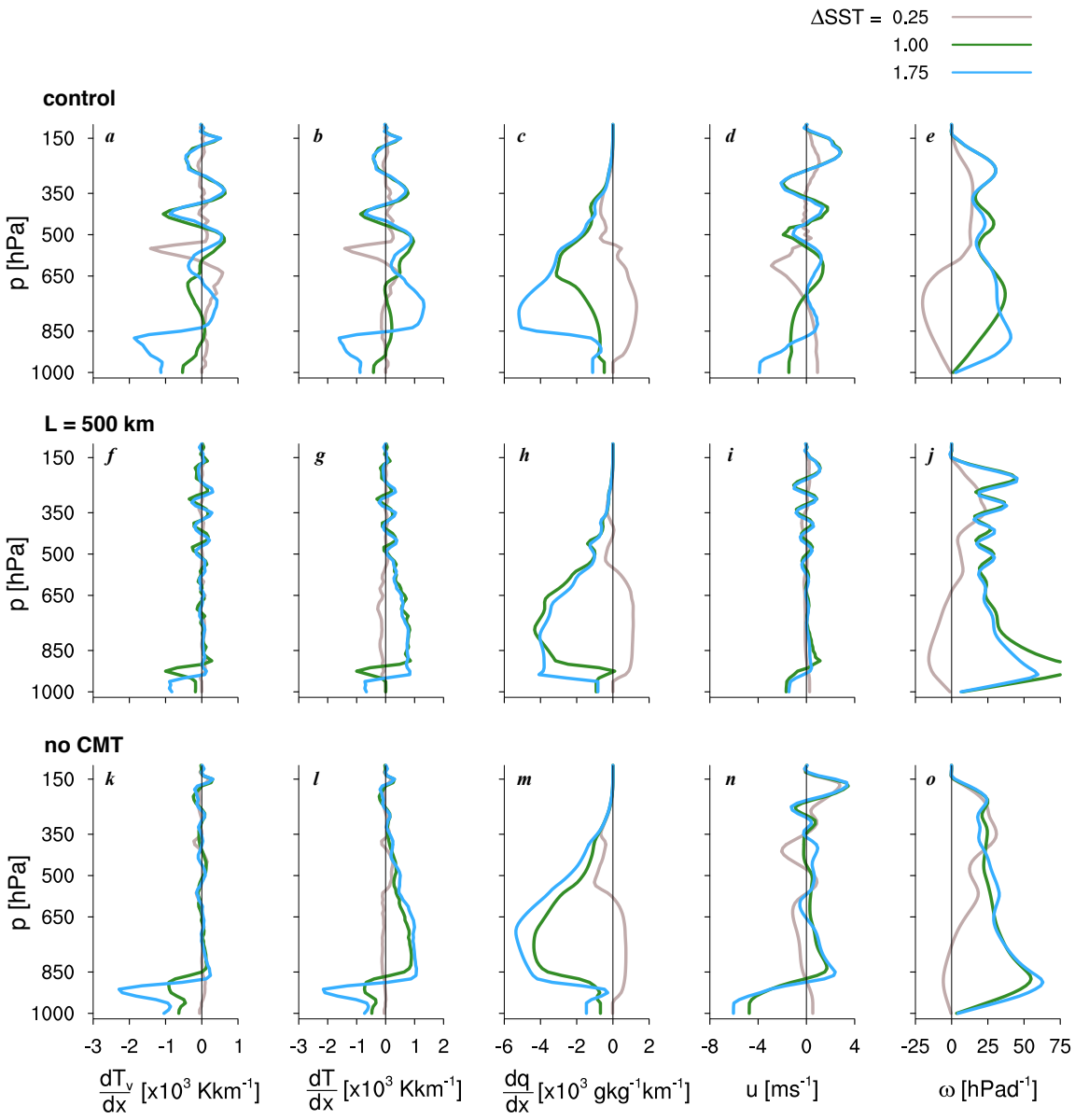

Figure 9. Profiles of the thermodynamic gradients and structure of the circulation over the cold SST column for the control run (top panels, similar to Figure 4), for a run with a smaller domain size of L =500 km (middle panels) and for a run in which CMT is turned off (bottom panels). For the L =500 km run, the gradients have been reduced by a factor of 6, corresponding to the reduction in domain size. Plotted are (from left to right): the virtual temperature (buoyancy) gradient between the two columns dT_v/dx; the temperature gradient dT/dx ; the specific humidity gradient dq/dx; the horizontal velocity u at the column boundary; and the vertical velocity over the cold ocean ω^{cold}.

The importance of CMT for convective tops can be seen when contrasting the runs with CMT for different domain sizes (Figure 8b) with runs in which CMT is turned off (Figure 8d). For example, using the control domain size ($L = 3000$ km, solid line) two of the congestus modes in green have become shallow modes when CMT is absent, and the deep and shallow modes are overall more unstable. The thermodynamic gradients and structure of the circulation for the 'no CMT' runs are shown in the bottom panels of Figure 9. These reveal that turning off CMT has a similar influence on the buoyancy gradient as using a smaller domain ($L = 500$ km): above 850 hPa, or above the tops of convection, buoyancy gradients have disappeared (Figure 9k) compared to the control run (Figure 9a). Without CMT both the blue and green runs also develop stronger near-surface winds and larger peaks in subsidence (Figures 9n and o), in response to stronger inversions near convective tops over the cold ocean (Figure 9l).

The zonal wind component of the circulation that develops is solved at column boundaries, but in the two-column system only one boundary exists: that between the two columns. Hence, CMT might have a stronger influence on the circulation than is realistic. Nevertheless, the runs illustrate that CMT might play an important role. Indeed, Kuang (2012) has demonstrated that the WTG assumption may be too stringent to reproduce mechanisms that help set the strength of mock Walker circulations, especially on large domains, which require larger temperature anomalies to drive the flow. Furthermore, Lin et al (2008) show that a strong mechanical damping is appropriate for models of tropical large-scale circulations, such as the Matsuno-Gill model, and that the structure of the damping is consistent with an eddy momentum flux by CMT.

The WTG approximation is typically only used above the boundary layer, precisely because of efficient momentum diffusion by turbulence. This is why even the runs without CMT can maintain temperature gradients between the two columns below 850 hPa (Figure 9k, l). The boundary layer depth (Δ_{PBL}) in which momentum diffusion takes place is 150 hPa in the control run. Because the convective tops of the shallow modes are near 850 hPa, Δ_{PBL} is suspected to play a role in setting these tops. However, if we decrease Δ_{PBL} to 70 hPa, the convective tops respond in a manner opposite to what one might expect: the tops of the shallow modes (blue)

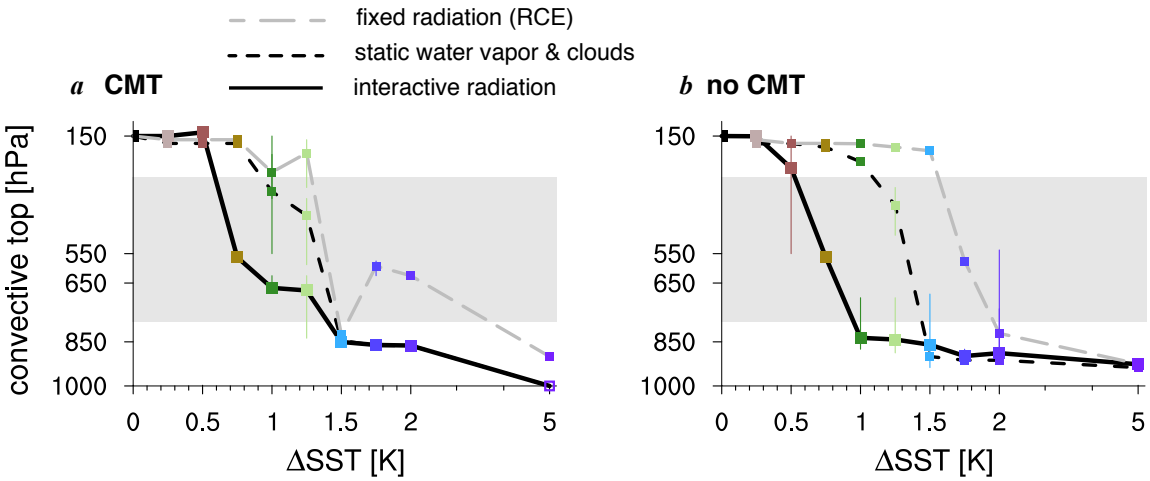

Figure 10. Convective tops over the cold ocean as a function of ΔSST, as in Figure 5a), but using different radiation calculations. The fully interactive radiation run (control case) is shown with a solid black line. Other runs use: fixed radiation (in dashed grey), whereby fixed means that a constant radiative cooling profile from the RCE state is imposed; and static water vapor and clouds, which means that the radiation scheme sees the water vapor and cloud profile from the RCE state, and only the temperature profile is interactive (in short dashed black).

and even a congestus mode (yellow) are raised instead of lowered (dashed lines in Figure 8c), and they become more unstable. If we instead raise Δ_{PBL} to 250 hPa, the tops of congestus are lowered, and the shallow tops do not change.

An explanation for this behaviour lies in the strength of the circulation, which is ultimately forced by the buoyancy gradient between the two columns. The total integrated buoyancy gradient increases as the depth Δ_{PBL} over which gradients are maintained increases. If we simplify Equation 3 by considering an equilibrium state ($\frac{\partial \eta}{\partial t} = 0$), ignoring advection, rotation and CMT, and assuming that the explicit damping is small compared to the momentum flux convergence in the boundary layer, a balance between the buoyancy gradient term and the momentum flux convergence must exist:

$$0 = \frac{\partial \alpha}{\partial x} + \frac{\partial \nu (\partial \eta / \partial p)}{\partial p} \tag{10}$$

The viscosity ν vanishes above the boundary layer. Hence, if we integrate from the surface p_s up to the top of the boundary layer $p_s - \Delta_{\mathrm{PBL}}$, and rearrange the stress term to the left hand side, we can write:

$$\nu_s \left(\frac{\partial \eta}{\partial p} \right)_s = \int_{p_s}^{p_s - \Delta \mathrm{PBL}} \frac{\partial \alpha}{\partial x} dp \tag{11}$$

The left hand side represents a measure of the strength of the circulation, *e.g.* the strength of the divergence in horizontal wind near the surface. By lowering Δ_{PBL} to 70 hPa, the circulation will weaken. The strong temperature gradients that exist near 850 hPa (Figure 9a) also weaken (not shown), which leads to less low-level subsidence over the cold ocean. In turn, this allows the shallow mode to deepen to congestus. But in absence of momentum dissipation above $p_s - \Delta_{\mathrm{PBL}}$ any gradients introduced by the deeper convection are hard to maintain, which results in an oscillation between shallow and congestus tops (Figure 8c).

If we compare the sensitivity of the tops of the shallow mode to different perturbations in Figures 5 and 8 (and to perturbations in the microphysics in the next section) we may conclude that shallow tops are strongly regulated by the circulation as set by the buoyancy gradient (and thus domain size) and the ability to sustain such a gradient through momentum diffusion in the lower atmosphere. Namely, the shallow tops are fairly robust, because the circulation introduces a negative feedback: an increase in the depth of the diffusive layer with a deepening of convection and the boundary layer leads to a larger buoyancy contrast, and therefore, stronger subsidence over the cold ocean, which in turn limits the depth of the diffusive layer. Only when the buoyancy gradients are changed independently of the convection, by changing the domain size, a significant change in the tops of the shallow mode is observed (Figures 8b and d).

But this does not explain why the tops of congestus, as long as enough momentum diffusion allows congestus to persist, are limited near 650-550 hPa. In the next section we discuss how interactive radiation and precipitation play a role at setting convective tops.

4.3. *Stabilizing role of radiation*

In section 3.2 we described how a circulating equilibrium develops from RCE, and mentioned the importance of a positive feedback between the developing circulation, a column drying and radiative cooling. Figure 10 shows how different radiation calculations influence convective tops over the cold ocean. In one set of runs, the radiation profile is fixed to that in RCE, and in another, radiation is calculated using the water vapor and cloud profiles fixed to that in RCE (static water vapor and clouds). In the latter, only temperature changes are seen by radiation. We also show the control runs with interactive radiation. Runs with CMT and without CMT are shown, which are qualitatively similar, except that the runs without CMT do not support congestus modes near 650 hPa.

Even when radiation is fixed (grey dashed lines) the convective tops over the cold ocean ultimately collapse. This happens at large ΔSSTs, when the surface fluxes become sufficiently small. But for ΔSSTs > 1.5 K convection still reaches mid-levels.

When only temperature interacts with radiation (black dashed lines) convection collapses sooner, and the shallow modes have somewhat lower convective tops. The dependence on temperature is important where inversions are present, such as at the mixed-layer top. As the SST is lowered and the inversion strength increases, the sub-cloud layer cools less radiatively. At large enough ΔSST this stabilisation at low levels apparently outweighs the effect of reduced emission at lower temperatures (which could theoretically relax the cooled column back to RCE).

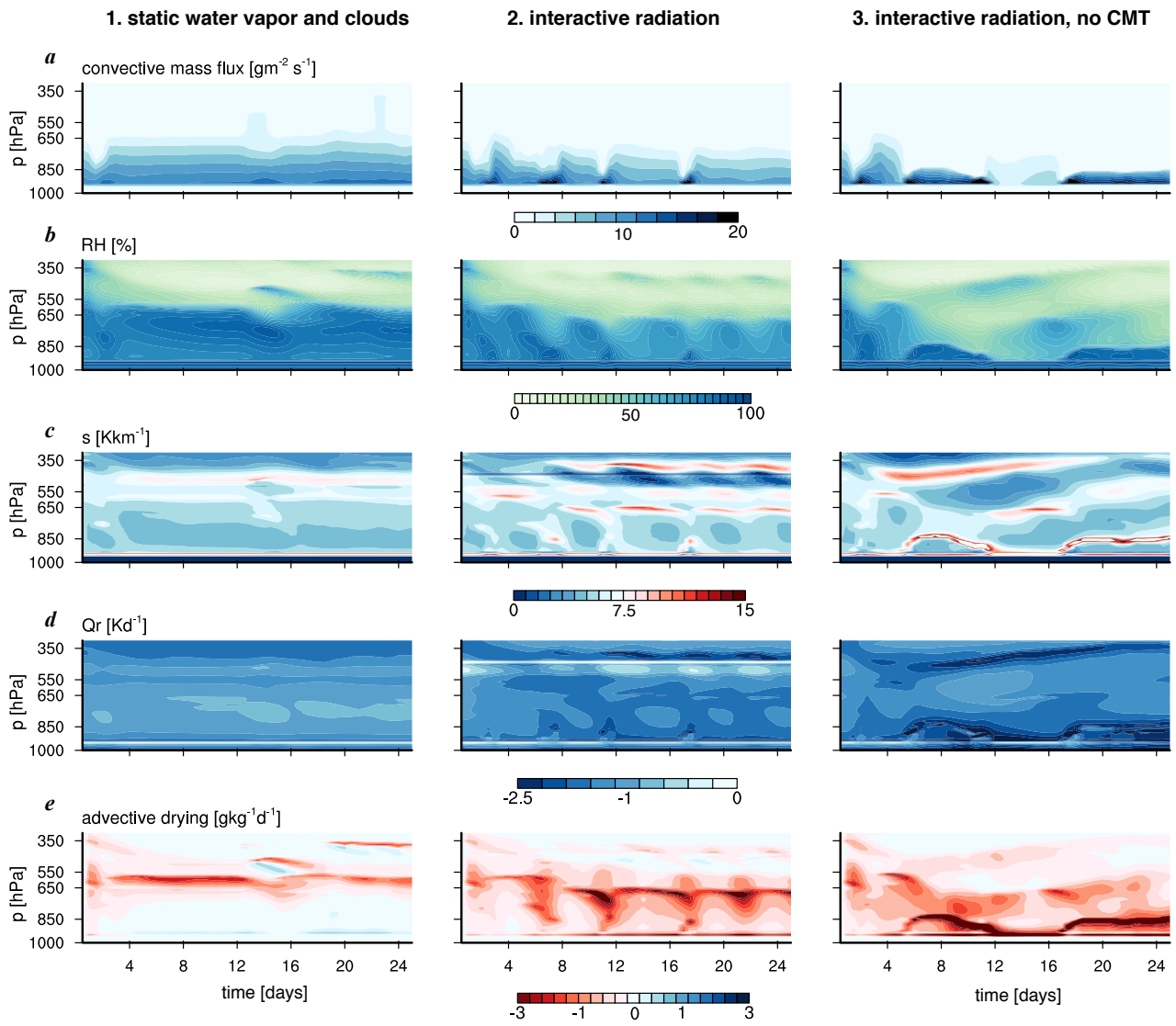

Figure 11. The evolution of the cold column during the first 30 days after lowering the SST from an RCE state. Contour plots are shown for the run with static water vapor and clouds, interactive radiation, and interactive radiation without CMT (see also Figure 10). Variables plotted are a) the convective mass flux, b) relative humidity, c) the static stability, d) radiative cooling and e) drying from vertical advection.

When water vapor and clouds do interact with radiation (black solid lines), convection collapses even sooner. Especially when the drying starts at upper levels, the moist lower atmosphere can radiate and cool effectively, triggering larger subsidence and further drying (Nilsson and Emanuel 1999). The stabilizing effect of moisture - radiation interactions is illustrated using Figure 11, which shows the thirty-day evolution of the convective mass flux, relative humidity, static stability, radiative cooling and advective drying over the cold ocean from RCE to a circulating equilibrium, here for ΔSST = 1.25K. From left to right we show the runs with static water vapor and clouds, with interactive radiation, and with interactive radiation but without CMT. The plotted evolution shows that convection in all three runs immediately collapses to about 650 hPa upon lowering the SST, which is at the level of neutral buoyancy (note that the 650 hPa level coincides with the base of a layer with somewhat larger stability already in RCE (Figure 11c)). This immediate collapse demonstrates just how important the SST and initial parcel buoyancy are at setting convective tops.

In the following days, interactions with radiation and the circulation allow convection to recover and get deeper (with static water vapor and clouds) or collapse even further (with interactive radiation). Subsidence initially has the shape of a first baroclinic mode with a maximum in the middle atmosphere, and dries upper levels (Figures 11b and e). In the static water vapor run this does not influence the radiative cooling profile (Figure 11c), whereas in the interactive radiation runs radiative cooling increases below 550 hPa and decreases at the base of a layer with low relative humidity between 550 - 450 hPa. This radiative cooling profile further increases the static stability near 550 hPa. Furthermore, and in contrast to the run with static water vapor, subsidence and subsidence drying increase throughout the lower atmosphere, and halt convective tops near 750-700 hPa. Over the next weeks convective tops in the interactive radiation runs oscillate between 650 and 850 hPa, which nicely demonstrate the response of subsidence drying to radiative cooling, which in turn responds to the moisture transported upwards by convection. An additional stable layer develops near convective tops at 650 hPa (Figure 3j). In the absence of such stabilizing mechanisms, convection in the static water vapor run can gradually deepen and eventually reach 350 hPa (Figure 10a).

The run without CMT has similar feedbacks between convective moistening, radiative cooling near cloud tops, and enhanced advective drying. But layers with pronounced radiative cooling and heating are more quickly dissipated by horizontal temperature advection, which caps the region of enhanced cooling, destabilisation and convection to 850 hPa.

5. Summary and discussion

We have used a two-column model to study equilibrium circulations and the depth of convection in the subsiding branch. The models solves for two-dimensional non-linear flow on a non-rotating sphere. Convection, clouds and radiation are parameterized, and the depth of convection in the subsiding branch is solved interactively, rather than set a-priori. Circulations are forced by imposing a range of SST gradients from a state of RCE in both columns. By using only two interacting columns on a non-rotating sphere we avoid the complex dynamics of GCMs. But even with this simplified set-up, the character of the circulating equilibrium is intricate, involving the interaction between many different processes.

The model produces a range of convective tops with increasing SST gradient that are reminiscent of the trimodal nature of convection found in nature and in cloud-resolving models (Johnson *et al.* 1999; Posselt *et al.* 2008; Mechem and Oberthaler 2013). While convection over the warm ocean continues to be deep, convection over the cold ocean collapses from deep convection (150 hPa) first to cumulus congestus (650 - 550 hPa), and then to shallow cumulus (850 hPa). The multiple modes of convection are an inherent feature of the models' convection scheme, which is independent of the vertical resolution.

A signature of the congestus and deep mode is already present in RCE. The model favours levels of neutral buoyancy and detrainment near the tropopause and at mid-levels, but not exactly at the freezing level. Similar detrainment levels occur in runs where discontinuities in precipitation and saturation vapor pressure across the freezing level are removed, and where radiation is non-interactive. Hence, the only explanation we can find for preferred mid-level detrainment is a minimum in radiative cooling at mid-levels, which accompanies the tropical temperature profile. Once detrainment occurs, it cools mid-levels, and lapse rates occasionally become super-adiabatic. This allows subsequent convection, once beyond congestus, to deepen without much further detrainment all the way to the tropopause. This keeps the atmosphere between the freezing level and the tropopause relatively dry. Interactive radiation then helps develop a stable layer at the base of this dry layer, at about 650 hPa.

This dry and stable layer set in RCE is maintained when a circulation develops, which dries upper levels. Detrainment of moisture near the tops of shallower convection also triggers radiative cooling, and leads to a peak in subsidence near the tops of convection. Without that interaction of water vapor with radiation, the congestus mode disappears. At low enough SSTs, the shallow mode exists without interactive radiation, whereas at higher SSTs, the interaction of radiation with a strong low-level inversion is needed.

The exact tops of the shallow mode are not very sensitive to changes in model physics, because they are strongly constrained through the circulation and the depth of the diffusive boundary layer, which is set to 850 hPa. The strength of the circulation namely depends on the depth of the boundary layer over which horizontal temperature gradients with the adjacent warm column can develop. Momentum diffusion in the boundary layer damps buoyancy waves, and therefore allows the formation of a temperature gradient, whereas above the boundary layer, horizontal gradients tend to vanish (the weak temperature gradient approximation). When the boundary layer deepens, in response to a deepening of shallow convection, the buoyancy contrast integrated over the boundary layer also increases, and the circulation will strengthen. The stronger subsidence will act to limit shallow convection: a negative feedback. The tops of the shallow mode therefore only change when the strength of the circulation is altered externally, such as by changing the domain size, or by changing the depth of the diffusive (boundary) layer. The depth of the shallow convective layer in nature no doubt depends on details of boundary layer physics, which are largely absent in this model.

This feedback involving the circulation is also important for congestus, which is overall far more delicate than the shallow mode. Congestus is accompanied with more convective heating and deeper moist layers, which reduce low-level radiative cooling. This weakens low-level subsidence, which in turn supports congestus. But congestus only develops when there is enough momentum diffusion above the boundary layer, such as on large-enough domains, or when having enough convective momentum transport (CMT). Congestus also collapses to a shallow mode when rain formation is less efficient (Nuijens *et al.* 2017).

Our results thus show that radiation, convection, cloud microphysics, and the circulation are all important at setting the depth of convection in the subsiding column. Furthermore, the depth of convection in the subsiding column has an influence on the character of deep convection in the ascending column. When congestus develops, near-surface winds are weaker, and the lower atmosphere stabilizes. Through horizontal advection, this stabilisation is also felt over the warm ocean, where cloud base mass fluxes and surface evaporation decrease. Although the tops of deep convection do not change, precipitation rates go down, and deep convection detrains more moisture on its way to the tropopause.

We also show that stable layers in the middle atmosphere may be created from processes other than freezing and melting, such as by dry and moist layers that result from deep convection, and which interact with radiation and the circulation, as other studies have suggested (Mapes and Zuidema 1996; Posselt *et al.* 2008). The structure of the circulation can therefore be complex. In some model set-ups, not just one or even two overturning cells are present, but three cells: a deep return flow in the upper atmosphere; a shallow return flow near the cool tops of shallow and congestus modes; and a return flow in the middle atmosphere, near the top of the dry layer over the warm ocean, where radiative cooling is small. This complex structure critically depends on the scale of the circulation, and the amount of momentum diffusion within the atmosphere.

Our study of course has limitations, most importantly, we use only two columns with equal sizes. Feedbacks involving the strength of subsidence are likely weaker when the subsiding branch of the circulation occupies a larger fraction of the domain. The results also no doubt strongly depend on the convection and cloud scheme that are used. Nevertheless, the results emphasize that besides cloudiness and radiative cooling, the depth of convection, and small-scale processes such as momentum diffusion play an important role in the character of overturning circulations, and are worth a deeper investigation using cloud-resolving models.

Acknowledgements

The first author would like to thank the EAPS department at MIT for hosting her as a postdoctoral fellow, and the Max Kade Foundation, the Max Planck Society, and Professors Reimar Lüst, Bjorn Stevens and Martin Claussen for their funding and support. Professor Chris Bretherton and Dr. Cathy Hohenegger are thanked for insightful discussions. The second author was supported by the National Science Foundation under grant AGS-1418508.

References

Bellon G, Treut HL. 2003. Large-scale and evaporation-wind feedbacks in a box model of the tropical climate. *Geophysical Research Letters* **30**(22): 2145.

Bony S, Emanuel KA. 2001. A Parameterization of the Cloudiness Associated with Cumulus Convection ; Evaluation Using TOGA COARE Data. *J. Atmos. S* **58**: 3158–3183.

Bretherton CS, Sobel AH. 2002a. A simple model of a convectively coupled walker circulation using the weak temperature gradient approximation. *Journal of Climate* **15**(20): 2907–2920.

Bretherton CS, Sobel AH. 2002b. A simple model of a convectively coupled walker circulation using the weak temperature gradient approximation. *Journal of Climate* **15**(20): 2907–2920.

Clement A, Seager R. 1999. Climate and the tropical oceans. *Journal of Climate* **12**(12): 3383–3401.

Emanuel KA, Zivkovic-Rothman M. 1999. Development and Evaluation of a Convection Scheme for Use in Climate Models. *J. Atmos. Sci* **56**: 1766–1782.

Fouquart Y, Bonnell B. 1980. Computation of solar heating of the Earth's atmosphere: A new parameterization. *Contrib. Atmos. Phys.* **53**: 35–62.

Hohenegger C, Stevens B. 2016. Coupled radiative convective equilibrium simulations with explicit and parameterized convection. *Journal of Advances in Modeling Earth Systems* **8**(3): 1468–1482.

Johnson RH, Rickenbach TM, Rutledge SA, Ciesielski PE, Schubert WH. 1999. Trimodal Characteristics of Tropical Convection. *Journal of Climate* **12**(8): 2397–2418.

Larson K, Hartmann DL, Klein SA. 1999. The role of clouds, water vapor, circulation, and boundary layer structure in the sensitivity of the tropical climate. *Journal of Climate* **12**(8 PART 1): 2359–2374.

Luo Z, Liu GY, Stephens GL, Johnson RH. 2009. Terminal versus transient cumulus congestus: A CloudSat perspective. *Geophysical Research Letters* **36**(5): 4–7.

Mapes BE, Zuidema P. 1996. Radiative-Dynamical Consequences of Dry Tongues in the Tropical Troposphere. *Journal of the Atmospheric Sciences* **53**(4): 620–638.

Mauritsen T, Stevens B. 2015. Missing iris effect as a possible cause of muted hydrological change and high climate sensitivity in models. *Nature Geosci* **8**(5): 346–351.

Mechem DB, Oberthaler aJ. 2013. Numerical simulation of tropical cumulus congestus during TOGA COARE. *Journal of Advances in Modeling Earth Systems* **5**(July): n/a–n/a.

Miller RL. 1997. Tropical thermostats and low cloud cover. *Journal of Climate* **10**(3): 409–440.

Morcrette JJ. 1991. Radiation and cloud radiative properties in the European Centre for Medium Range Weather Forecasts forecasting system. *Journal of Geophysical Research: Atmospheres* **96**(D5): 9121–9132.

Muller CJ, Held IM. 2012. Detailed Investigation of the Self-Aggregation of Convection in Cloud-Resolving Simulations. *Journal of the Atmospheric Sciences* **69**(8): 2551–2565.

Naumann AK, Stevens B, Hohenegger C, Mellado JP. 2017. A Conceptual Model of a Shallow Circulation Induced by Prescribed Low-Level Radiative Cooling. *Journal of the Atmospheric Sciences* **74**(10): 3129–3144.

Neggers RAJ, Neelin JD, Stevens B. 2007. Impact Mechanisms of Shallow Cumulus Convection on Tropical Climate Dynamics*. *Journal of Climate* **20**(11): 2623–2642.

Nilsson J, Emanuel K. 1999. Equilibrium atmospheres of a two-column radiative-convective model. *Quarterly Journal of the Royal Meteorological Society* **125**: 2239–2264.

Nuijens L, Emanuel K, Masunaga H, L'Ecuyer T. 2017. Implications of Warm Rain in Shallow Cumulus and Congestus Clouds for Large-Scale Circulations. *Surveys in Geophysics* .

Nuijens L, Medeiros B, Sandu I, Ahlgrimm M. 2015. Observed and modeled patterns of covariability between low-level cloudiness and the structure of the trade-wind layer. *Journal of Advances in Modeling Earth Systems* **7**(4): 1741–1764.

Pakula L, Stephens GL. 2009. The Role of Radiation in Influencing Tropical Cloud Distributions in a RadiativeConvective Equilibrium Cloud-Resolving Model. *Journal of the Atmospheric Sciences* **66**(1): 62–76.

Pauluis O, Emanuel K. 2004. Numerical Instability Resulting from Infrequent Calculation of Radiative Heating. *Monthly Weather Review* **132**(3): 673–686.

Peters ME, Bretherton CS. 2005. A simplified model of the Walker circulation with an interactive ocean mixed layer and cloud-radiative feedbacks. *Journal of Climate* **18**(20): 4216–4234.

Pierrehumbert RT. 1995. Thermostats, Radiator Fins, and the Local Runaway Greenhouse. *Journal of the Atmospheric Sciences* **52**(10): 1784–1806.

Posselt DJ, van den Heever SC, Stephens GL. 2008. Trimodal cloudiness and tropical stable layers in simulations of radiative convective equilibrium. *Geophysical Research Letters* **35**(8): L08 802.

Raymond DJ, Blyth AM. 1986. A Stochastic Mixing Model for Nonprecipitating Cumulus Clouds. *Journal of the Atmospheric Sciences* **43**(22): 2708–2718.

Riehl H, Yeh TC, Malkus JS, la Seur NE. 1951. The north-east trade of the Pacific Ocean. *Quarterly Journal of the Royal Meteorological Society* **77**(334): 598–626.

Sherwood SC, Bony S, Dufresne JL. 2014. Spread in model climate sensitivity traced to atmospheric convective mixing. *Nature* **505**(7481): 37–42.

Sobel AH, Neelin JD. 2006. The boundary layer contribution to intertropical convergence zones in the quasi-equilibrium tropical circulation model framework. *Theoretical and Computational Fluid Dynamics* **20**(5-6): 323–350.

Sun DZ, Liu Z. 1996. Dynamic Ocean-Atmosphere Coupling : A Thermostat for the Tropics. *Science* **272**(5265): 1148–1150.

Tiedtke M. 1989. A comprehensive mass flux scheme for cumulus parameterization in large-scale models. *Monthly Weather Review* **117**: 1779–1800.

Vial J, Bony S, Dufresne JL, Roehrig R. 2016. Coupling between lower-tropospheric convective mixing and low-level clouds: Physical mechanisms and dependence on convection scheme. *Journal of Advances in Modeling Earth Systems* **8**(4): 1892–1911.

Wing AA, Emanuel KA. 2014. Physical mechanisms controlling self-aggregation of convection in idealized numerical modeling simulations. *Journal of Advances in Modeling Earth Systems* **6**(1): 59–74.

Zhang C, Nolan DS, Thorncroft CD, Nguyen H. 2008. Shallow meridional circulations in the tropical atmosphere. *Journal of Climate* **21**(14): 3453–3470.